Boundary-Layer Meteorol (2008) 128:103–116
DOI 10.1007/s10546-008-9277-y

NOTE

Local Similarity in the Stable Boundary Layer and Mixing-Length Approaches: Consistency of Concepts

B. J. H. van de Wiel · A. F. Moene · W. H. De Ronde · H. J. J. Jonker

Received: 3 September 2007 / Accepted: 6 May 2008 / Published online: 3 June 2008

Abstract In stably stratified flows vertical movement of eddies is limited by the fact that kinetic energy is converted into potential energy, leading to a buoyancy displacement scale z_B. Our new mixing-length concept for turbulent transport in the stable boundary layer follows a *rigid-wall analogy*, in the sense that we assume that the buoyancy length scale is similar to neutral length scaling. This implies that the buoyancy length scale is: $\ell_B = \kappa_B z_B$, with $\kappa_B \approx \kappa$, the von Karman constant. With this concept it is shown that the physical relevance of the local scaling parameter z/Λ naturally appears, and that the α coefficient of the log-linear similarity functions $\phi_{m,h} = 1 + \alpha z/\Lambda$ is equal to c/κ^2, where c is a constant close to unity. The predicted value $\alpha \approx 1/\kappa^2 = 6.25$ lies within the range found in observational studies. Finally, it is shown that the traditionally used inverse linear interpolation between the mixing length in the neutral and buoyancy limits is inconsistent with the classical log-linear stability functions. As an alternative, a log-linear consistent interpolation method is proposed.

Keywords Mixing length · Local similarity · Stable boundary layer

1 Introduction

1.1 Monin–Obukhov Theory

The chaotic nature of turbulence prevents exact analytical solutions to describe turbulent transport in the atmospheric boundary layer. Instead, the cornerstone of the description of turbulent exchange near the surface is based on Monin–Obukhov (MO) similarity theory

B. J. H. van de Wiel (✉) · A. F. Moene
Department of Meteorology and Air Quality, Wageningen University and Research Centre, Droevendaalsesteeg 4, 6708 PB Wageningen, The Netherlands
e-mail: Bas.vandeWiel@wur.nl

W. H. De Ronde · H. J. J. Jonker
Department of Multi-Scale Physics, Delft University of Technology, Lorentzweg 1, 2628 CJ Delft, The Netherlands

(Monin and Obukhov 1954; see also: Businger and Yaglom 1971; Obukhov 1971). This predicts 'universal' relations for the dimensionless gradients of the velocity U and temperature θ in terms of the dimensionless height parameter z/L,

$$\frac{\partial U}{\partial z}\left(\frac{\kappa z}{u_{*0}}\right) = \phi_m = f_m\left(\frac{z}{L}\right), \tag{1}$$

$$\frac{\partial \theta}{\partial z}\left(\frac{\kappa z}{\theta_{*0}}\right) = \phi_h = f_h\left(\frac{z}{L}\right) \tag{2}$$

with u_{*0} the surface friction velocity and θ_{*0} the surface temperature scale ($\theta_{*0} \equiv -\overline{w'\theta'}_0/u_{*0}$), and where κ is the von Karman constant and $L \equiv (\theta/(\kappa g))(u_{*0}^2/\theta_{*0})$, the Obukhov length scale. Because surface fluxes are used, (1) and (2) are valid only in the atmospheric surface layer.

1.2 Monin–Obukhov Versus Local Similarity

For the stable boundary layer a solid physical basis for (1) and (2) was found by Nieuwstadt (1984). He showed that the relevant dimensionless groups need not come from dimensional analysis alone, but can be inferred from a physical model, by analyzing parameterized equations for the turbulent variances and covariances. This finally leads to a system of seven coupled algebraic equations with eight unknown dimensionless groups. Consequently, specification of one of the groups fixes the other groups. Thus all dimensionless combinations can be expressed in terms of a single parameter z/Λ and for the dimensionless gradients of wind and temperature he obtained:

$$\frac{\partial U}{\partial z}\left(\frac{\kappa z}{u_*}\right) = \phi_m = f_m\left(\frac{z}{\Lambda}\right), \tag{3}$$

$$\frac{\partial \theta}{\partial z}\left(\frac{\kappa z}{\theta_*}\right) = \phi_h = f_h\left(\frac{z}{\Lambda}\right), \tag{4}$$

where Λ is the local Obukhov length, expressed in terms of local fluxes u_* and θ_*, $\Lambda \equiv (\theta/(\kappa g))(u_*^2/\theta_*)$. As such (3) and (4) are generalizations of (1) and (2), because they are also valid outside the surface layer. Though very elegant, the approach of Nieuwstadt (1984) uses a rather complex system of coupled equations (with specific closure assumptions on mixing lengths, to be discussed in Sect. 4). The physical relevance of z/Λ can also be found more easily from simple mixing-length considerations, as will be shown in the present work.

1.3 The 'Log-Linear Law'

For weak to moderate stability (say $z/\Lambda < O(1)$) observational studies, see e.g. Högström (1996), suggest a linear character of the stability functions in (3) and (4):

$$\phi_m = 1 + \alpha_m \frac{z}{\Lambda}, \tag{5}$$

$$\phi_h = 1 + \alpha_h \frac{z}{\Lambda}, \tag{6}$$

so that wind and temperature profiles show so-called *'log-linear behaviour'*. In the literature, $\alpha_{m,h}$ typically ranges from 4 to 8 (Högström 1996, and references herein). Contrary to

the results for weak stability, observational studies diverge considerably for large stability $z/\Lambda > O(1)$, so that presently there is no conclusive result on ϕ_m or ϕ_h in this range (Mahrt 1999). This lack of 'universality' may be due to a number of factors, including:

- In strong stratification fluxes are often very weak and intermittent (Mahrt 1999), so that it is difficult to obtain accurate flux estimates from the observations (flux errors strongly affect z/Λ, because Λ scales as $1/u_*^3$ (Baas et al. 2006).
- With non-stationarity and horizontal heterogeneity, and as fluxes become small, the relative contribution of non-stationary mesoscale fluxes to the total turbulent flux increases, which makes the results very sensitive to the time-averaging procedure (Vickers and Mahrt 2006). Generally speaking, non-stationarity causes a 'leveling-off' of ϕ_m and ϕ_h (Mahrt 2007).
- Non-turbulent processes, such as gravity-wave transport and longwave radiative cooling, become more important as stability increases.

A new theoretical perspective (A.F. Moene, personal communication 2008) uses direct numerical simulation (DNS: Appendix A) of the Navier–Stokes equations for stably stratified flow with a relatively low Reynolds number ($O(10^4)$, compared to Re in the atmospheric stable boundary layer $O(10^8)$). The study found strong evidence for 'Re-similar' flow with results apparently insensitive to the large difference in Re. From this, it was concluded that similarity relations such as (3) and (4) could be determined directly from the DNS, with its obvious advantage over observations with respect to stationarity and homogeneity. We summarize the DNS results with respect to Eqs. 3 and 4 in Fig. 1.

A clear linear dependence appears over a large stability range ($0 < z/\Lambda < 5$), and although a marginal difference between ϕ_m and ϕ_h is found, both curves seem to be rather well represented by the function $\phi_{m,h} = 1 + 4.5\, z/\Lambda$, which implies a turbulent Prandtl-number ≈ 1.0. As such this study supports log-linear dependence over a large stability range in an 'idealized stationary, homogeneous atmosphere'. We note that re-analysis of Fig. 1 for non-stationary cases (not shown) clearly showed a leveling-off, an effect that is well-known for atmospheric studies on the non-stationary stable boundary layer (SBL), (Mahrt 2007).

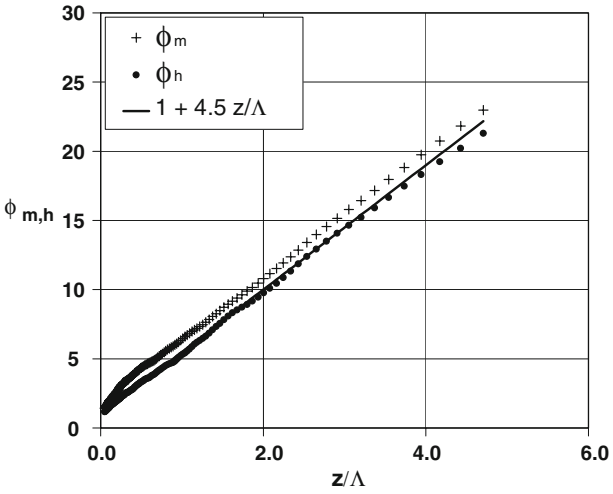

Fig. 1 Dimensionless gradients as a function of the stability parameter z/Λ, as obtained from DNS (see: Appendix A). For comparison the line $\phi_{m,h} = 1 + 4.5 z/\Lambda$ is given

The $\alpha_{m,h}$ coefficient (4.5) lies within the atmospherically observed range $4 \leq \alpha_{m,h} \leq 8$ (Högström 1996); we later provide a physical reason for this particular $\alpha_{m,h}$ range, based on mixing length considerations.

As characteristics of the ϕ functions can be inferred from mixing-length considerations, the reverse is also true: observed ϕ functions may help determine mixing length approaches that are consistent with atmospheric observations. As such, both concepts are inherently connected, and an interesting study on a similar connection in relation to closure constants in the turbulent kinetic energy (TKE) equation was given recently by Baas et al. (2008). We illustrate our point by referring to the well-known classical approach to find the master length scale from simple inverse linear interpolation between the neutral and the buoyancy length scales:

$$\frac{1}{\ell} = \frac{1}{\ell_N} + \frac{1}{\ell_B}. \tag{7}$$

Although this approach is both practically attractive and provides the correct physical limits it lacks observational evidence, and it is unclear why Eq. 7 should be preferred over inverse quadratic or other interpolation methods. In fact, we show below that the inverse linear interpolation in (7) is *inconsistent* with a log-linear behaviour of the ϕ functions, and we provide an alternative fully consistent interpolation.

2 Local Scaling from a Mixing-Length Model: A Rigid-Wall Analogy

2.1 Basic Assumptions

We adopt a rigid wall analogy for the buoyancy length scale and show that the physical relevance of the stability parameter z/Λ directly follows from a mixing-length approach. The following assumptions are made:

(1) *Validity of K-theory*: this implies that local fluxes can be related directly to the local gradients of the mean variables.
(2) *The turbulent diffusivities for heat and momentum: we assume* $K_h = K_m$

Assumption (1) is often made in the stable boundary layer since non-local transport of turbulent kinetic energy is usually small in stably stratified conditions (Derbyshire 1999). Without a priori knowledge, (2) is assumed for simplicity. With (1) the momentum and heat fluxes can be expressed as:

$$u_*^2 = K_t \frac{\partial U}{\partial z}, \tag{8}$$

$$\theta_* u_* = K_t \frac{\partial \theta}{\partial z}, \tag{9}$$

where K_t is modelled in terms of velocity and length scales:

$$K_t = u_* \ell. \tag{10}$$

Note that *local fluxes* and *ensemble averaged variables* are used unless stated otherwise. Now the problem is reduced to finding the correct length scale ℓ.

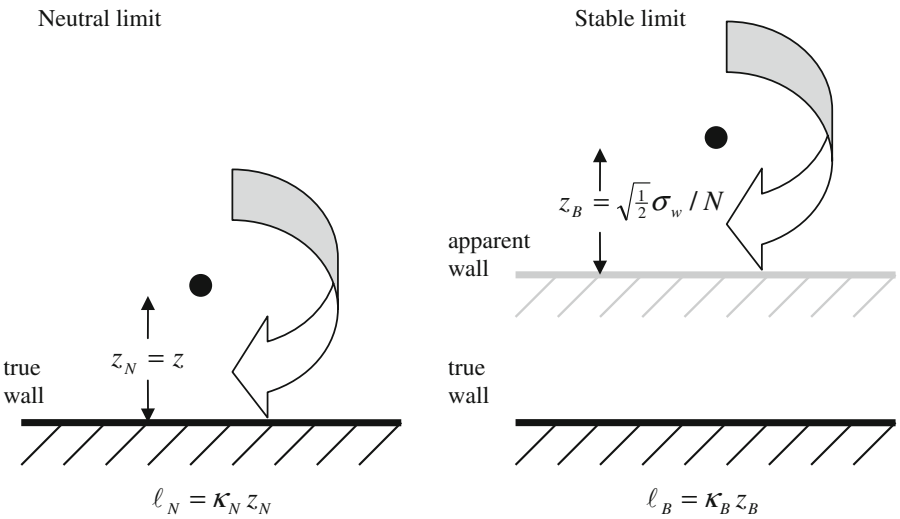

Fig. 2 The buoyancy length scale from an apparent rigid wall perspective

2.2 The Rigid-Wall Analogy

The governing length scale of turbulence closure is related to the displacement of turbulent eddies, and in the neutral limit the displacement of eddies is limited by the distance to the wall (Fig. 2). At maximum the displacement equals the height z, but on average, the displacement will be less than this maximum. From observations in neutral conditions, the turbulent length scale is directly related to the maximum displacement by:

$$\ell_N = \kappa_N z_N = \kappa z \tag{11}$$

with κ the von Karman constant. Equation 11 is well-founded in the fluid mechanics literature (Kundu 1990), and in accordance with vast observational evidence we take $\kappa = 0.4$.

Also in the limit of extreme stratification it is possible to define a typical length scale: the buoyancy length scale. To this end we first derive a maximum displacement height z_B, which is considered to be the distance between the level under consideration and an apparent 'wall' (Fig. 2). Then by analogy to neutral wall flows the buoyancy length scale is readily found via: $\ell_B \equiv \kappa_B z_B$ (where the subscribt 'B' indicates 'buoyancy').

The maximum displacement height is diagnosed from energy conservation arguments. Due to energy conservation, the vertical displacement of an eddy is limited by stratification (Brost and Wyngaard 1978, Hunt et al. 1985) and maximum displacement is reached when all vertical kinetic energy of the eddy motion is transferred into potential energy (frictionless): $\Delta E_{POT} = -\Delta E_{KIN}$. The mean vertical kinetic energy of the eddies (per volume) is represented by $\frac{1}{2}\rho\sigma_w^2$ and potential energy that can be gained due to 'Archimedes-effects' is $|\Delta\rho|\, z_B g$, with z_B the displacement (defined as a positive number), and $\Delta\rho$ the difference in density between the final and the reference height. Thus:

$$|\Delta\rho|\, z_B g = \frac{1}{2}\rho\sigma_w^2, \tag{12}$$

and with the Boussinesq approximation we replace density variations by temperature variations: $|\Delta\theta/\theta_0|\, z_B g = \frac{1}{2}\sigma_w^2$. $|\Delta\theta|$ is replaced by $z_B \partial\theta/\partial z$ (in the stable limit, profiles are

approximately linear), and finally, an expression for the maximum displacement (apparent wall distance) z_B is found:

$$z_B = \sqrt{\frac{1}{2}}\left(\frac{\sigma_w}{N}\right), \tag{13}$$

with $N^2 = (\partial\theta/\partial z)(g/\theta_0)$, N being the buoyancy frequency. Next, we eliminate σ_w, by using the fact that all dimensionless groups have to reach constant values in the strong stability limit (Nieuwstadt 1984, Basu et al. 2006). Hence we have $\sigma_w = Cu_*$, with C a proportionality constant, which leads to:

$$z_B = \sqrt{\frac{1}{2}}C\left(\frac{u_*}{N}\right). \tag{14}$$

Now, from the rigid-wall analogy, we assume, as with neutral wall flows, the buoyancy mixing length is directly related to the 'wall' distance via $\ell_B = \kappa_B z_B$:

$$\ell_B = \kappa_B\sqrt{\frac{1}{2}}C\left(\frac{u_*}{N}\right). \tag{15}$$

Below it will be shown that the physical relevance of z/Λ directly follows from this length scale.

2.3 From Buoyancy Length Scale to z/Λ

First, we combine (8) and (10) and (15) :

$$u_*^2 = K_t\frac{\partial U}{\partial z} = \kappa_B u_* z_B\frac{\partial U}{\partial z} = \kappa_B u_*\sqrt{\frac{1}{2}}C\frac{u_*}{N}\frac{\partial U}{\partial z}. \tag{16}$$

In (16) the temperature gradient can be replaced by a wind speed gradient, using (8) and (9). Then, after isolating the wind speed gradient, we have:

$$\left(\frac{\partial U}{\partial z}\right)\frac{\kappa z}{u_*} = \left(\frac{2}{\kappa_B^2 C^2}\right)\frac{z\theta_*}{u_*^2}\left(\frac{\kappa g}{\theta}\right) = \left(\frac{2}{\kappa_B^2 C^2}\right)\frac{z}{\Lambda} \tag{17}$$

and the scaling behaviour at the stable limit is now identical to the classical log-linear limit with the constants related as:

$$\left(\frac{2}{C^2}\right)\frac{1}{\kappa_B^2} = \alpha. \tag{18}$$

In this way the local Obukhov length is derived from a physical length-scale model.

3 Predicting the Value of α

In principle, α in (5) and (6) is a free constant that can only be determined from experiment. On the other hand, with the physical model above (Eq. 18), it is possible to obtain a direct estimate of α, by using (empirical) information on the ratio σ_w/u_*.

(A) From atmospheric and wind-tunnel observations and large-eddy simulations, Basu et al. (2006) show that σ_w/u_* is rather close to the value 1.4–1.5 at the large stability limit (and in fact surprisingly constant with respect to stability). Here, for simplicity, we take $C = \sigma_w/u_* \approx \sqrt{2}$, so that $C^2 = 2$.

(B) A true analogy of buoyancy as a 'pseudo-wall' effect implies that: $\kappa_B \approx \kappa_N = \kappa$. The consequence of this statement is evaluated below.

With assumptions (A) and (B) the value of α becomes: $\alpha = 1/\kappa^2 = 6.25$. This first-order estimate lies well within the observed range of 4 to 8 (Sect. 1).

In principle, assumption (B) gives an upper bound estimate for α (lower bound for κ_B). This can be understood by considering the fact that in neutral wall flows turbulence has a typical three-dimensional character as compared to the more two-dimensional character of turbulence in the stably stratified case. As such, the vortex-stretching mechanism and the energy dissipation is more effective in the first case. Consequently, the reduction of the mixing length when compared to the wall distance is somewhat larger in neutral than in stably stratified cases ($\kappa_B \geq \kappa_N$). On the other hand, the direct analogy $\kappa_B \approx \kappa_N$ seems to give realistic α values and so the difference between κ_B and κ_N cannot be too large.

The α value of 6.25 has implications in terms of the turbulent kinetic energy equation. First, it can be shown (Sect. 5) that α is related to the critical Richardson number via $1/\alpha = Ri_C = Rf_C$, the critical flux Richardson number (as before, we assume $K_h = K_m$). Thus $\alpha = 6.25$ implies $Rf_C = 0.16$, which in turn implies that in the stable limit 84% of the turbulent kinetic energy by shear production is still dissipated by internal friction. This 84% is not very different from the 100% under neutral conditions: changes due to the effect of buoyancy on the *relative* importance of the terms in the turbulent kinetic energy budget (as compared to the total shear production), seem to be small. Of course the *absolute magnitude* of all terms is strongly affected by stability.

In other words: all terms in the TKE budget equation are affected by the fact that z_B decreases strongly with stability, but the efficiency κ_B remains rather constant, i.e. close to its neutral value. The a posteriori argument of small perturbations in the TKE budget could be related to the fact that σ_w/u_* is rather constant with respect to stability, though this is difficult to prove from first principles.

Our concept also provides a direct quantitative link between the apparent wall distance z_B and the local Obukhov length Λ: $z_B = \Lambda/\alpha$, a useful rule of thumb. With B) this statement immediately implies: $\phi_{m,h} = z/z_B$, in the stable limit and in our framework (5) and (6) simply become: $\phi_{m,h} = 1 + z/z_B$.

Related to this, an interesting result was mentioned by Derbyshire (1990, his Fig. 1) who found a "*close association between the local Obukhov length* Λ *and the vertical displacement scale*". From LES simulations he found that the vertical profiles of σ_w/N were virtually identical to profiles of $\Lambda/5$. Thus $\sigma_w/N \approx \Lambda/5$, whereas our analysis predicts $\sigma_w/N \approx \Lambda\kappa^2/\sqrt{1/2} = \Lambda/4.4$, which is surprisingly close to the LES findings.

4 ϕ Functions and Interpolation of Mixing Lengths: Consistency of Concepts

4.1 A Physical Picture

Both the neutral and the buoyancy length scales ℓ_N and ℓ_B have to be combined in a single master length scale ℓ in order to arrive at flux-profile relationships. In order to derive a mathematical form of such a relationship, we use physical arguments based on the schematic in Fig. 2, which shows the *virtual* maximum eddy size due to separate wall and buoyancy effects. It is clear that the *actual* maximum size will be determined by the most limiting process, i.e. by the smallest maximum, leading to wall-limited size close to the wall and buoyancy limited size higher up.

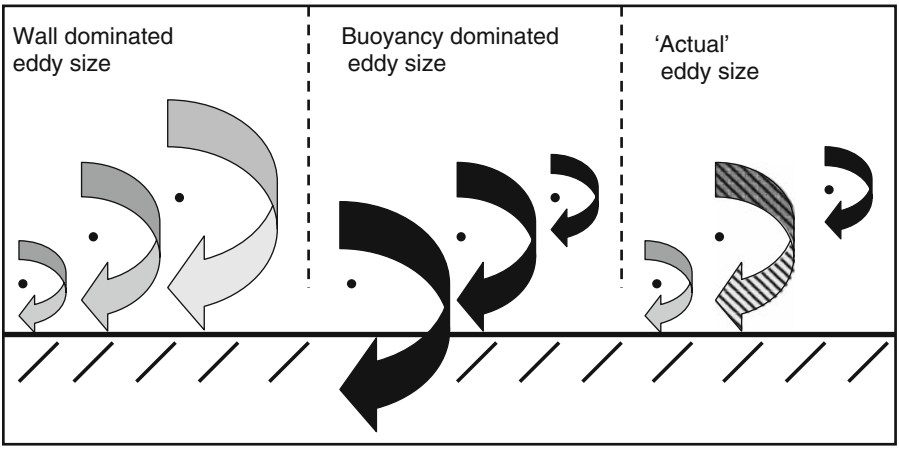

Fig. 3 'Actual' maximum eddy size as a combined result of wall (grey) and buoyancy (black) effects. In the first two frames *virtual* eddies are drawn. Note that the virtual, large eddy in the second frame only indicates that buoyancy is non-limiting near the ground. The actual eddy close to the ground is limited by wall effects (grey eddy, third frame). The dashed eddy is limited by both wall and buoyancy effects

Also, at a certain height both limiting effects are equally important. From the analysis above it is clear that the cross-over occurs at $z = z_N = z_B$, i.e. at $z/\Lambda = 1/\alpha$, and with the physical picture of Fig. 3, a natural way to combine ℓ_N and ℓ_B in ℓ is by inverse interpolation:

$$\frac{1}{\ell^\delta} = \frac{1}{\ell_N^\delta} + \frac{1}{\ell_B^\delta}, \tag{19}$$

where the exponent δ is a free parameter. Now consider the extreme case: $\delta \to \infty$. In this limit $\ell = MIN(\ell_N, \ell_B)$ as in the simplified picture in Fig. 3. In reality however, it is more likely that *both* wall and buoyancy effects become relevant once they are of comparable magnitude, so that there is a smoother transition between both processes. This is achieved by choosing a lower value for δ. In virtually all studies reported δ is set equal to 1 yielding inverse linear interpolation (e.g. Brost and Wyngaard 1978, Nieuwstadt 1984):

$$\frac{1}{\ell} = \frac{1}{\ell_N} + \frac{1}{\ell_B} \tag{20}$$

whose consequences for ϕ are evaluated below. By inserting (20) in (16) it can be shown (Appendix B) that inverse linear interpolation implies:

$$\phi_{m,h} = 1 + \frac{1}{2}\alpha\frac{z}{\Lambda} + \frac{1}{2}\left(\left(\alpha\frac{z}{\Lambda}\right)^2 + 4\left(\alpha\frac{z}{\Lambda}\right)\right)^{\frac{1}{2}}, \tag{21}$$

which is not the traditional log-linear ϕ function. Consequently, the traditional interpolation in (20) seems to deviate from observational evidence. As an alternative, it is tempting to take the observed ϕ functions as a point of departure and then find the interpolation function from inverse calculation. Such alternative interpolation would have a direct foundation in observational data. If we start with the log-linear ϕ functions $\phi_{m,h} = 1 + \alpha z/\Lambda$ this leads to (Appendix B):

$$\frac{1}{\ell_{TOT}} = \frac{1}{2\ell_N} + \left(\frac{1}{4\ell_N^2} + \frac{1}{\ell_B^2}\right)^{\frac{1}{2}}. \tag{22}$$

This interpolation between ℓ_N and ℓ_B should be used in mixing length studies if one aims to represent the log-linear stability functions.

4.2 Consistency of Concepts

In the section above the mixing-length concept and the concept of similarity functions were linked. We could go one step further by also taking into account the flux-gradient relations that use the stability functions based on the gradient Ri number $f(Ri)$, since all these concepts apply to K-theory:

$$K_t = \ell^2 \frac{\partial U}{\partial z}, \tag{23a}$$

$$K_t = \ell_N^2 \frac{1}{\varphi_{m,h}^2} \frac{\partial U}{\partial z}, \tag{23b}$$

$$K_t = \ell_N^2 f(Ri) \frac{\partial U}{\partial z}, \tag{23c}$$

with $Ri \equiv (g/\theta_0)\,(\partial\theta/\partial z)\,/\,(\partial U/\partial z)^2$. All these concepts should in principle be fully equivalent (Derbyshire 1999), and in Table 1 the relationships between the three concepts for specific choices of the formulations are shown. In this way the consequences of a certain choice in the mixing-length formulation are immediately clear and explicit. The results of Table 1 are visualized in Fig. 4a, b.

From Fig. 4a it appears that (at first glance) the three alternative mixing-length formulations of Table 1 produce similar $\phi_{m,h}$. The log-linear consistent relation lies in between the inverse linear and inverse quadratic interpolation (and is not very different from an inverse 3/2-power interpolation, i.e. $\delta = 3/2$). However, Fig. 4b shows that the impact of the mixing-length formulation is significant. This paradox is resolved by realizing that:

(a) In Fig. 4a differences are significant for z/Λ smaller than say 0.5;
(b) $z/\Lambda = 0.5$ already corresponds to $\alpha Ri \approx 0.7$ (using $\alpha \approx 5$), i.e. almost the full scale in Fig. 4a.

So, figures with a large scale on the z/Λ axis (as in Fig. 1) can be misleading from a Ri perspective.

Table 1 Assumed mixing-length formulations with explicit consequences for $\phi_{m,h}$ and $f(Ri)$

MO log-linear consistent	Inverse linear (classical)	Inverse quadratic
$\frac{1}{\ell_{TOT}} = \frac{1}{2\ell_N} + \left(\frac{1}{4\ell_N^2} + \frac{1}{\ell_B^2}\right)^{\frac{1}{2}}$	$\frac{1}{\ell_{TOT}} = \frac{1}{\ell_N} + \frac{1}{\ell_B}$	$\frac{1}{\ell_{TOT}^2} = \frac{1}{\ell_N^2} + \frac{1}{\ell_B^2}$
$\phi_{m,h} = 1 + \alpha \frac{z}{\Lambda}$	$\phi_{m,h} = 1 + \frac{1}{2}\alpha \frac{z}{\Lambda} + \frac{1}{2}\sqrt{\left(\alpha \frac{z}{\Lambda}\right)^2 + 4\left(\alpha \frac{z}{\Lambda}\right)}$	$\phi_{m,h} = \frac{1}{2}\alpha \frac{z}{\Lambda} + \frac{1}{2}\sqrt{\left(\alpha \frac{z}{\Lambda}\right)^2 + 4}$
$f(Ri) = (1 - \alpha Ri)^2$	$f(Ri) = (1 - \sqrt{\alpha Ri})^2$	$f(Ri) = (1 - \alpha Ri)$

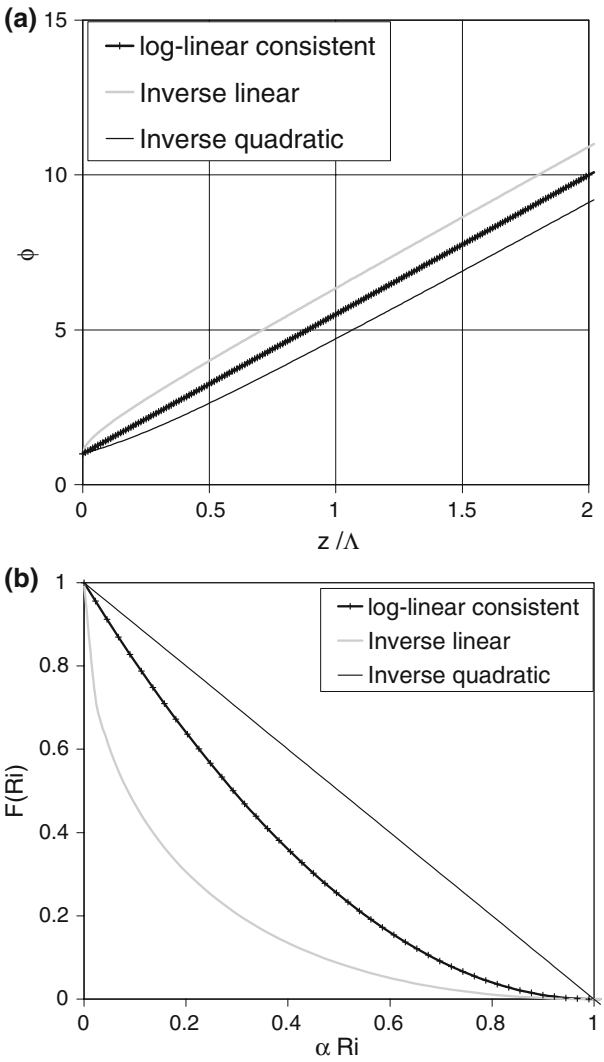

Fig. 4 **(a)** Graphical presentation of the $\phi_{m,h}$ functions in Table 1 (here $\alpha_{m,h} = 4.5$). **(b)** Graphical presentation of the $f(Ri)_{m,h}$ functions in Table 1

5 Discussion

5.1 Mixing-Length Interpolation

At this point it goes beyond the scope of this text to discuss all the observational evidence for the particular mixing-length formulation to be used. Nevertheless, some comments are made below. In our analysis, the DNS results do not a priori exclude either the log-linear consistent or the inverse linear interpolation (compare Figs. 1 and 4a). However, for consistency (e.g. with the Businger–Dyer formulations) the slightly more complex method is preferred over the traditional interpolation method. At this point we mention that the inverse quadratic interpolation does not seem to be supported by typical atmospheric observations (compare Fig. 4b with observations by Duynkerke and De Roode 2001).

As mentioned in the introduction, since Nieuwstadt (1984) some studies have used higher order turbulence closure models to arrive at explicit local-scaling functions. Often, the choice of closure constants is discussed at length, but not the choice of mixing-length formulation itself. In the present work we show that this latter choice is not trivial, and deserves validation against observational data in order to give physically reliable results.

5.2 The Critical Richardson Number

From Table 1 it appears that no turbulent flux exists whenever $Ri \geq 1/\alpha = Ri_c$. This conclusion is also elegantly derived by considering equation (16) in the stable limit (Derbyshire, personal communication, 2007):

$$\frac{u_*}{\partial U/\partial z} = \ell_B = \kappa_B \sqrt{\frac{1}{2}} \sigma_w / N, \tag{24}$$

which can be written as:

$$Ri = \frac{1}{2} \kappa_B^2 (\sigma_w / u_*)^2. \tag{25}$$

Thus, in the stable limit Ri reaches a constant, denoted as $Ri_c = \frac{1}{2}\kappa_B^2(\sigma_w/u_*)^2 = 1/\alpha$, due to (18). However, it must be realized that the existence of a critical Ri is a direct consequence of our assumption $\mathrm{Pr}_t \approx 1$. This analogy between momentum and heat is non-trivial in the sense that pressure–gradient fluctuations can play a systematic role. This is an important difference in the equations governing u'(and hence K_m) as opposed to θ' (and hence K_h).

For this reason the Ri_C issue remains an open question and the physics behind the critical Richardson number concept is still under debate (Zilitinkevich et al. 2007, Van de Wiel et al. 2007). On the other hand, we note that $\mathrm{Pr}_t \approx 1$ is supported by our DNS results in the stable limit (Fig. 1). In the case of $\mathrm{Pr}_t \neq 1$ the analysis could be extended without loss of generality.

6 Conclusions

From the present work the following conclusions are drawn:

- The physical relevance of the local scaling parameter z/Λ naturally appears from the buoyancy length scale by following a mixing length approach using a rigid wall analogy. As such we support the findings of Derbyshire (from LES simulations) that $\Lambda \propto \ell_B$.
- With the present approach an estimation for the 'free' parameter α in the flux-gradient relationships can be anticipated based on physical arguments: $\alpha = 2/((\sigma_w^2/u_*^2)\kappa^2) \approx 1/\kappa^2 = 6.25$. This value lies within the range reported in observational studies.
- The full mixing length approach requires some interpolation between the mixing length in the neutral and the buoyancy limits: ℓ_N and ℓ_B. It is shown that the classical inverse linear interpolation is inconsistent with the classical log-linear stability functions. As an alternative, a log-linear consistent interpolation method is proposed.

Acknowledgements We very much appreciate the suggestions of Steve Derbyshire on an earlier version of the manuscript. Also our colleagues Prof. Bert Holtslag and Dr. Gert-Jan Steeneveld are acknowledged for providing useful comments.

Appendix A: Some Characteristics of Direct Numerical Simulation

Our model results in Fig. 1 result from a direct numerical simulation (DNS), which, in principle, does not need subgrid modelling of turbulence as does large-eddy simulation. Instead, the Navier–Stokes equations are solved directly in their discretized form. The flow configuration is similar to that in Nieuwstadt (2005): a stably stratified smooth channel flow with height h. In the present simulation the characteristic forcing parameters are $Re_* = u_{*0}h/\nu = 720$ (as opposed to $Re_* = 360$ in Nieuwstadt) and $h/L = 0.4$ (defined with the Von Karman constant in L contrary to the definition in Nieuwstadt). Here u_{*0} is a forcing parameter based on the pressure gradient: $u_{*0} \equiv \sqrt{-(1/\rho)\,(\partial P/\partial x)\,h}$. A frictional Reynolds number equal to 720 implies a bulk Reynolds number O(14000). Elaborate studies showed that the flow was very similar to atmospheric stratified flow. Further characteristics of the simulation are:

- Periodic boundary conditions in the x and y directions.
- Boundary conditions in the z direction.
  - Prescribed temperature at the channel top.
  - Prescribed surface heat flux.
  - No slip at the surface and free slip at the channel top.
  - Zero vertical velocity at top and bottom.
- 200^3 grid cells and a domain size of $5h$ in the x and y directions and h in the z directions.
- Pressure gradient forcing in the x direction.

The simulation was run for $102t_*$ (with $t_* = h/u_*$), and the results of Fig. 1 are based on statistics derived from fields from the last $2t_*$. Implementation details of the model are similar to those of the LES model used in Moene (2003): second-order finite volume discretization in space and the second-order Adams–Bashforth method is used for time integration. Features not used in the present simulation comprise system rotation around an arbitrary axis, gravity working in an arbitrary direction, periodic boundary conditions in the z direction and forcing of velocities and scalars with a linear gradient (useful for the simulation of homogeneous turbulence).

Appendix B: Derivations

We provide a general derivation to find consistent $\varphi_{m,h}$ and $f(Ri)$ from the mixing-length interpolation for any δ. The specific cases from Table 1 ($\delta = 1, 2$) can be found directly from this solution. Realizing that $u_* = \ell\partial U/\partial z$, the following relations are found from K-theory:

$$\left(\frac{\ell_B}{\ell}\right)^2 = \tilde{k}_B^2 \frac{1}{Ri}, \tag{26}$$

$$\left(\frac{\ell_B}{\ell}\right)^2 = \tilde{k}_B^2 \frac{\varphi}{(z/\Lambda)}. \tag{27}$$

For convenience we defined $\tilde{k}_B^2 \equiv (1/2)C^2\kappa_B^2$. From $K_t = \ell^2\partial U/\partial z = \ell_N^2 f(Ri)\partial U/\partial z$ and φ:

$$f(Ri) = (\ell/\ell_N)^2, \tag{28}$$

$$\varphi = \ell_N/\ell. \tag{29}$$

- From length scales to $f(Ri)$ and φ

The general interpolation $1/\ell^\delta = 1/\ell_N^\delta + 1/\ell_B^\delta$ is rewritten as:

$$\left(\frac{\ell}{\ell_B}\right)^\delta + \left(\frac{\ell}{\ell_N}\right)^\delta = 1, \tag{30}$$

and with (26) and (28) we write (30) in terms of $f(Ri)$:

$$f(Ri) = \left(1 - \left(\frac{Ri}{Ri_c}\right)^{\delta/2}\right)^{2/\delta}. \tag{31}$$

With, as before, $Ri_c = \tilde{k}_B^2 = 1/\alpha$. Likewise with (27) and (29), (30) becomes:

$$\left(\frac{z/\Lambda}{\varphi \tilde{k}_B^2}\right)^{\delta/2} + \varphi^{-\delta} = 1, \tag{32}$$

and after multiplication by φ^δ, one can solve a second-order equation in $\varphi^{\delta/2}$ yielding:

$$\varphi = \left(\frac{\left(\alpha \frac{z}{\Lambda}\right)^{\delta/2} + \sqrt{\left(\alpha \frac{z}{\Lambda}\right)^\delta + 4}}{2}\right)^{2/\delta}. \tag{33}$$

- *From φ to $f(Ri)$ and ℓ*

With $\phi = 1 + \alpha z/\Lambda = 1 + (1/\tilde{k}_B^2) z/\Lambda$ inserted in (27), and using (29):

$$\left(\frac{\ell_B}{\ell}\right)^2 = \frac{\varphi}{\varphi - 1} = \frac{\ell_N}{\ell_N - \ell}. \tag{34}$$

This result may be rewritten as a second-order equation in $1/\ell$, which yields the interpolation formula given in the main text (Eq. 22). In terms of Ri we have((26), (27) and (34)): $\alpha\varphi/(\varphi - 1) = 1/Ri$ or $\varphi = 1/(1 - \alpha Ri)$, which via (28) and (29) gives:

$$f(Ri) = (1 - \alpha Ri)^2 = (1 - Ri/Ri_c)^2. \tag{35}$$

References

Baas P, Steeneveld GJ, Van de Wiel BJH, Holtslag AAM (2006) Exploring self-correlation in flux-gradient relationships for stably stratified conditions. J Atmos Sci 63:3045–3054

Baas P, De Roode SR, Lenderink G (2008) The scaling behaviour of a turbulent kinetic energy closure model for stably stratified condtions. Boundary-Layer Meteorol 127:17–36

Basu S, Porté-Agel F, Foufoula-Georgiou E, Vinuesa J-F, Pahlow M (2006) Revisiting the local scaling hypothesis in stably stratified atmospheric boundary layer turbulence: an integration of field and laboratory measurements with large-eddy simulations. Boundary-Layer Meteorol 119:473–500

Brost RA, Wyngaard JC (1978) A model study on the stably stratified planetary boundary layer. J Atmos Sci 35:1427–1440

Businger JA, Yaglom AM (1971) Introduction to Obukhov's paper on 'Turbulence in an atmosphere with a non-uniform temperature'. Boundary-Layer Meteorol 2:3–6

Derbyshire SH (1990) Nieuwstadt's stable boundary layer revisited. Quart J Roy Meteorol Soc 116:127–158

Derbyshire SH (1999) Stable boundary layer modelling: established approaches and beyond. Boundary-Layer Meteorol 90:423–446

Duynkerke PG, De Roode SR (2001) Surface energy balance and turbulence characteristics observed at the SHEBA ice campe during FIRE III. J Geophys Res 106:15313–15322

Högström U (1996) Review of some basic characteristics of the atmospheric surface layer. Boundary-Layer Meteorol 78:215–246

Hunt JCR, Kaimal JC, Gaynor JE (1985) Some observations of turbulence structure in stable layers. Quart J Roy Meteorol Soc 111:793–815

Kundu PK (1990) Fluid mechanics. Academic Press, San Diego, 638 pp

Mahrt L (1999) Stratified atmospheric boundary layers. Boundary-Layer Meteorol 90:375–396

Mahrt L (2007) The influence of nonstationarity on the turbulent flux–gradient relationship for stable stratification. Boundary-Layer Meteorol 125:245–264

Moene AF (2003) Swirling pipe flow with axial strain: experiment and large eddy simulation. PhD thesis, Technical University Einhoven, ISBN 90-386-1695-3, 237 pp

Monin AS, Obukhov AM (1954) Basic laws of turbulent mixing in the atmosphere near the ground. Tr Akad Nauk SSSR Geophiz Inst 24 151:1963–1987

Nieuwstadt FTM (1984) The turbulent structure of the stable, nocturnal boundary layer. J Atmos Sci 41:2202–2216

Nieuwstadt FTM (2005) Direct numerical simulation of stable channel flow at large stability. Boundary-Layer Meteorol 116:277–299

Obukhov AM (1971) Turbulence in an atmosphere with a non-uniform temperature. Boundary-Layer Meteorol 2:7–29

Van de Wiel BJH, Moene AF, Steeneveld GJ, Hartogensis OK, Holtslag AAM (2007) Predicting the collapse of turbulence in stably stratified boundary layers. Flow Turbulence Combust 79:251–274

Vickers D, Mahrt L (2006) A solution for flux contamination by mesoscale motions with very weak turbulence. Boundary-Layer Meteorol 118:431–447

Zilitinkevich SS, Elperin T, Kleeorin N, Rogachevskii I (2007) Energy- and flux-budget (EFB) turbulence closure model for stably stratified flows. Part I: steady state, homogeneous regimes. Boundary-Layer Meteorol 125:167–191